4.1 Introduction

Since the publication of the first organic semiconductor-based transistor in 1986, organic electronics have advanced significantly [297]. Organic semiconductors and devices offer a wide range of structural diversity [298,299], lowered temperature functionality [300], low-cost manufacturing, significant production, and adaptability for researchers. It is not just the conducting material of organic nature itself that determines an OFET device's functioning, but also additional components such as semiconductor/dielectric interfaces [301]and contact interfaces [302,303]. The efficiency of OFET devices has been reported to be quickly growing after decades of material research and manufacturing process development, and carrier mobility requirements are increased continuously [304,305]. Researchers have developed improved organic semiconductor materials for organic field-effect transistor (OFET) applications as well as a variety of other devices that rely on charge transfer, such as organic solar cells [306] and light-emitting devices [307].

Polymer composites have proved their promise as high-performance and versatile materials, making them one of the most fascinating and investigated fields in nanotechnology and composites. The features of the polymer matrix, such as low density and flexibility, can be integrated with the mechanical or other physical qualities of the filler by embedding a filler into the polymer matrix [308,309]. The electrical percolation threshold is frequently lowered by raising the filler aspect ratio. [310,311]. In this regard, due to its exceptional electrical, mechanical, and physical capabilities, graphene, a two-dimensional carbon framework with a single-atom thickness, has attracted a lot of attention [266]. Few layers and single-layer graphene flakes are predicted to offer a good link between the crystalline areas of the semiconductor sheet. The peculiar properties of graphene resulted in an ambipolar electric field effect, with holes and electron concentrations of up to 10^{13} cm^{-2} and around 15,000 cm^2 V^{-1}s^{-1} mobility even in ambient settings [312,313]. Researchers are attempting to combine graphene into the polymer matrix to form graphene-polymer nanocomposites for these reasons. For specialised device assembly, a few layers of graphene were originally generated via mechanical exfoliation of graphite [38] and epitaxial chemical vapour deposition [134], but they are not appropriate for large-scale manufacture. Graphene can be produced in bulk form using chemical methods. The most frequent method is graphite exfoliation via graphite

oxidation, which results in graphite oxide, which is held together by Vanderwall forces between graphene oxide layers [135-137]. Graphene oxide contains a carbon structure that is comparable to graphene, but it also has oxygen functional groups [138]. Because of its hydrophilicity, GO is an excellent material for forming a homogeneous thin layer in electronics [139,140]. Through the use of an appropriate reduction technique, GO can be converted into reduced graphene oxide, which resembles pure graphene in terms of characteristics and has fewer oxygen functional groups [141,314]. Although there are still many issues with the restoration of graphitic structure [315]. The growing curiosity about conductive reduced graphene oxide (rGO) composites stems from the requirement for the systematic production of durable graphene-based electrically conductive polymer composites.

Polythiophene derivatives based on conjugated polymers, such as poly(3-hexylthiophene) (P3HT), Poly[5,5′-bis(3-dodecyl-2-thienyl)-2,2′-bithiophene] (PQT), and Poly(2,5-bis(3-alkylthiophen-2-yl)thieno[3,2-b]thiophene) (PBTTT), are promising materials for fabricating OFETs [316] due to their efficient solution forming skill, high charge carrier movement, and low-cost compatibility with random supporting base (such as paper, plastic, glass, silicon, etc. PBTTT is chosen over other conjugated polymers for a variety of applications due to its increased air stability and carrier mobility. Alkyl side chains and π-π stacking help build a self-organized, structured framework with better charge transport. Now, to make use of the distinctive attributes of two-dimensional rGO nanosheets and the conjugated polymer PBTTT, we've chosen these two materials for OFET fabrication and are constructing a thin film of the hybrid nanocomposite. It is important to note that the practical use of these nanocomposite materials in large-area, wearable electronic devices is strongly related to the capacity to generate materials at much lower costs than standard electronic device design. The creation of an organic semiconductor active layer is an important stage in the manufacture of OFETs and other electronic devices.[317]. As a consequence, a deposition method that provides for precise control of molecular/chain ordering, film morphology, and crystalline orientation of semiconducting material is very preferable [318]. Researchers have previously used a variety of methods, such as rubbing, the Langmuir-Blodgett technique and the self-organization of liquid crystals to control the properties of conjugated polymers [319-322]. Although these processes are complex and need the knowledge to obtain improved molecular or polymer chain organisation, these techniques are time- and effort-efficient

in the long run. The "Floating Film Transfer Method (FTM)"[323] is a simple technique for lifting a polymer film from a hydrophilic liquid surface to produce an aligned polymer film. Despite the lack of surface-pressure application, the floating film transfer process suggested here is comparable to one for laying Langmuir-Sheffer (LS) film.

In this report, we have synthesized rGO from GO nanosheets by thermal reduction. Afterwards, PBTTT/rGO nanocomposite is synthesized by ultrasonication and stirring and developed into a thin film on a hydrophilic phase by the floating film transfer method. The as-deposited film's morphological, structural, spectroscopic, and electrochemical properties were contrasted to those of a pure polymer film. The polymer nanocomposite film was employed to fabricate thin film transistors and displayed enhanced device performance under ambient conditions.

4.2 Results and Discussion

4.2.1 Characterization of GO and rGO nanosheets

XRD spectrum of graphene oxide designates peak at 10.1˚ with (001) diffraction plane of graphene oxide, while a broad hump in the XRD pattern of rGO occurs at 25.01˚ which corresponds to (002) plane and a small peak occurs at 43˚ for (100) plane is shown in Fig.4.1(a)(i, ii). The interlayer distance rGO is found to be 0.36 nm($2\theta=25.01˚$) with the help of Braggs law $\lambda=2d\sin\theta$, where λ is X-ray wavelength. Closed rGO spacing and disappearance of the peak at $2\theta= 10.1°$ imply oxygen functional group elimination. Reduced graphene oxide(rGO) nanosheets' surface morphology is studied by HRSEM and TEM (Fig.4.1(b)and (c)).HRSEM image of rGO sheets shows haphazardly aggregated and rippled thin sheets having wrinkled and folded structures. However, the TEM image of rGO sheets shows sheet-like structures with different transparencies because of different overlapped layers. The transparencies are due to the oxidation of graphene sheets which helps in exfoliation in monolayers. The rGO nanosheet shows corrugated structures due to the disorder of the sp^2 hybridised graphitic region by the introduction of different oxygen functionalities(sp^3 hybridized carbon).It is thought that secluded oxidized areas formed on the GO surface with most of the graphitic region intact.By reduction, oxidized areas are converted back to the sp^2 hybridized carbon network. Reduction causes rGO lack of orderliness of graphene sheet in terms of topological defects(isolated and clustered), strain and plane deformations (in and out).

The TEM image of rGO is corrugated and curly. It is because corrugation and scrolling are the inherent nature of GO and rGO, as the 2D structures become stable thermodynamically via bending [324].The SAED pattern used to characterize the crystallinity of nanomaterial shows a ring-like pattern in rGO. The diffused rings in SAED in the inset of Fig.4.1(c) occurred due to the sp^3 carbon atom formed during oxidation with the graphitic island intact which is because of the loss of extended order between graphene sheets.Fig.4.1(d) shows the HR-TEM image of rGO lattice fringes with an inset having an FFT profile of lattice spacing of 0.36nm. Since the GO is thermally reduced it removes oxide functionality and therefore interplanar spacing decreases close to pristine graphite.In addition, restacking of GO sheets in rGO on thermal reduction causes the number of layers to increase in comparison to GO [325]. This is further supported in the Raman spectrum of GO and rGO while calculating the number of layers(I_{2D}/I_G ratio).Also, the FTIR spectrum of GO and rGO is depicted in Fig. 4.1(e)(i, ii). A broad peak in GO at 3400 cm^{-1} is attributed to O-H stretching frequency from intercalated water(H_2O), carboxylic (COOH) and alkoxy(C-OH) groups present at the edges of GO. There is a significant broadening in the O-H band due to water molecules embedded between graphene layers. However in rGO a visible reduction in the O-H bond. This is because of the vaporization of H_2O molecules present. The intense band at 1740 cm^{-1} is due to C=O stretching vibration from carbonyl (C=O) and the carboxyl group (COOH). While in rGO there is a decrease in intensity of the C=O band at 1730 cm^{-1} because of partial removal of the COOH group. Clusters of in-plane C=C bonds may be liable for the band at 1624 cm-1 in GO, which may be owing to intercalated water molecules. The peak intensity in rGO at 1624 cm^{-1} decrease may be due to the removal of the aromatic C=C bond so decrement in the size of the aromatic C=C domain and water molecule. Peaks at 1054 cm^{-1} and 1227 cm^{-1} in GO occur due to C-OH and C-O-C(epoxide) stretching vibrations. While in rGO C-OH and C-O-C (epoxide), peak intensities decrease due to the removal of residual hydroxyl(C-OH), carboxyl(COOH), and epoxide (C-O-C) groups. Raman spectrum of GO and rGO is shown in Fig.4.1(f)(i, ii) is the most used tool to characterize graphene-type material. The graphitic G band of pristine graphite occurs at 1580 cm^{-1} which corresponds to the first ordered scattered E2g mode sp^2 bonded graphitic region. In GO the G band is broad and shifted to a high wavenumber i.e. 1600 cm^{-1}. According to the literature, this upshift is because of the resonance of isolated double bonds in comparison to graphite [326] Also, there is another

peak arises at 1360 cm^{-1} i.e. D band which is A1g mode breathing vibrations occur due to the introduction of amorphous carbon (disordered) and shrinkage in the size of in-plane sp^2 bonded carbon network. This may be due to the extensive oxidation of graphite sheets. While in rGO the D and G bands occur at 1350 and 1590 cm^{-1} respectively. The ratio of intensities of D and G bands is used to determine the presence of structural defects and the size of the in-plane sp^2 lattice. The I_D/I_G ratio in GO is 0.89 while in rGO ratio is 0.93. The increased ratio is due to the increase of disordered regions in the sp^2 domain with additional structural defects upon thermal reduction [327].Although their re-establishment of the C=C bond leads to increased electrical conductivity. The G' or 2D band of GO and rGO occurred at around 2704 cm^{-1} and 2709 cm^{-1}.The number of layers in GO and rGO is calculated by I_G/I_{2D} ratio and is found at 11 and 14 respectively.
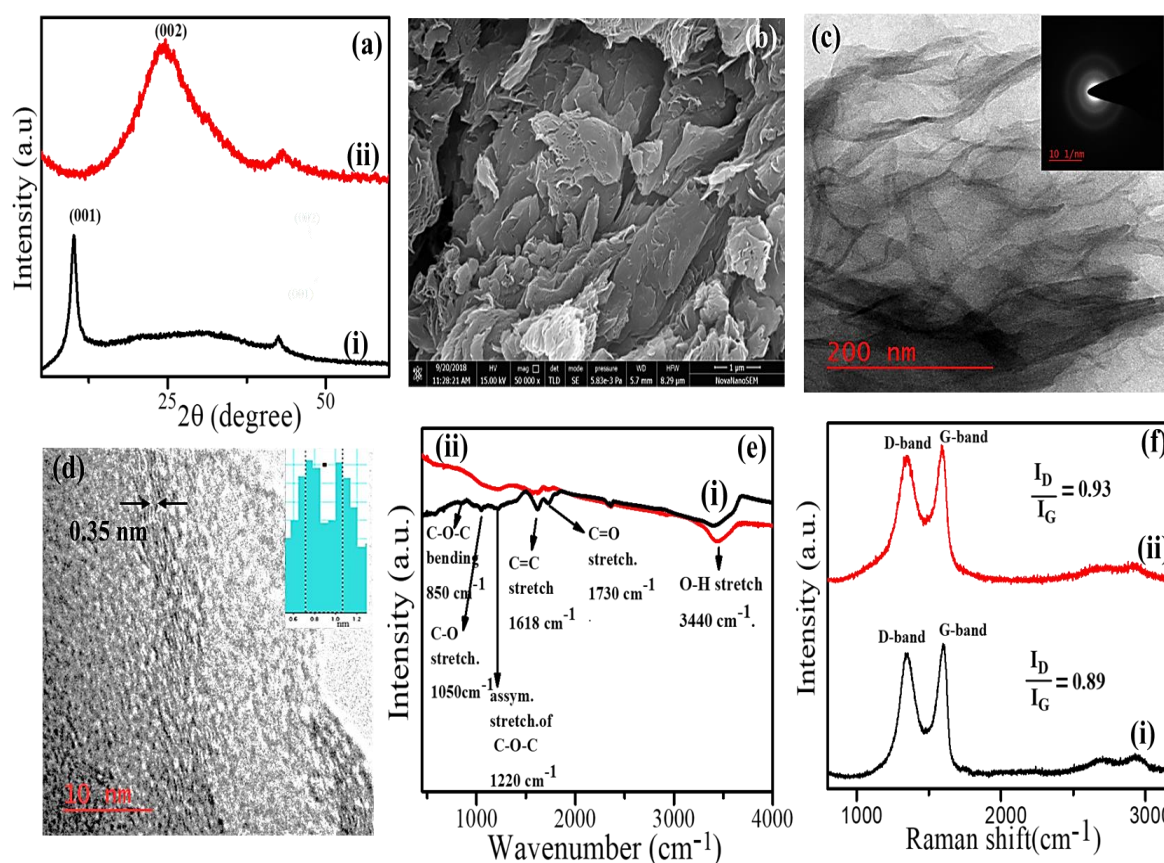
Fig.4.1 XRD pattern of (a) GO(i) and rGO(ii).(b) HRSEM images of GO(i) and rGO (ii).(c)TEM images of GO(i) and rGO(ii).(d)UV-VIS of GO(i) and rGO (ii).(e)FTIR of GO(i) and rGO(ii).(f)Raman of GO(i) and rGO (ii).

4.2.2 Characterization of PBTTT /rGO nanocomposite film

4.2.2.1 Morphological characteristics

Fig.4.2(a-d) shows TEM imaging of pure PBTTT and PBTTT/rGO nanocomposite films on a Cu grid (a-d). In Fig.4.3 (a), the TEM study of a pure polymer film displays a folded structure, whereas the composite FTM film exposes rGO in the PBTTT polymer framework(Fig.4.2(b-d)). As a result, the decorating of the PBTTT polymer nanostructure over rGO sheets is evident in the TEM pictures.HR-TEM of the same (Fig. 4.2(d)) only shows the (010) plane, which corresponds to π-π stacking. Brinkmann et al. developed highly oriented, crystalline polymer films with edge-on lamellar structures [286]. The d–spacing of the (0 1 0) plane or the π-π stacking distance of PBTTT backbones corresponds to the lattice fringe separation of 0.39 nm. For in-plane devices like transistors, the anisotropic nature of polymer makes it ideal to have a lamellar structure of polymer backbones that are edge-on across the substrate. In addition, the presence of diffused rings in the SAED graph of PBTTT/rGO film (inset of Fig. 4.2(d)) substantiates the fact that the PBTTT/rGO film is of a polycrystalline structure. The AFM topographical, phase image and KPFM photos (scan area 5 µmx5 µm) of pristine PBTTT (Fig.4.2(a-c))and PBTTT/rGO(Fig.4.2(d-f)) thin film created by the FTM technique are presented in Fig. 4.3. The AFM topographical of both films reveal clear morphological differences (Fig. 4.3(a & d)), with bigger domains for the PBTTT/rGO nanocomposite having an average area roughness of 1.53 nm. This rather little change is the result of rGO nanosheets being present in the polymer matrix. Additionally, since a pure polymer medium does not include rGO sheets, smaller zones are formed. These zones may be either solitary or connected by unstructured long polymer chains, both of which reduce the material's conductivity and mobility. Phase imaging was used to evaluate the films' properties, which confirmed the observable phase difference for both films with different phase angles with an average roughness of PBTTT/rGO film found to be 1.772°. As in AFM topography, there are noticeable variations in phase pictures with the appearance of rGO sheets covered with polymer. It's worth noting that the topographical, phase picture and KPFM image were all taken at the same time. As a consequence, we decided to make use of KPFM to determine the surface potential microscopy (SPC) of the film in the same region as is represented in Fig. 4.3. As can be observed in Fig. 4.3(c and f), the contact potential difference of the surface of the two different films are not the same. A uniform

surface potential of 1.694 mV is shown by the KPFM image of the PBTTT/rGO film measured. This indicates that there is no barrier height between the nanosheets and the polymer aggregates [274]. Because of the broader domain and existence of nanosheets, there is a variance in SPC height and average SPC for both films. The average roughness in topography, phase and KPFM image of the pristine polymer film is found to be 1.371nm, 1.484 ° and 1.554 mV respectively. The small increment in the roughness value in PBTTT/rGO film may be due to the presence of rGO nanosheets in the polymer.
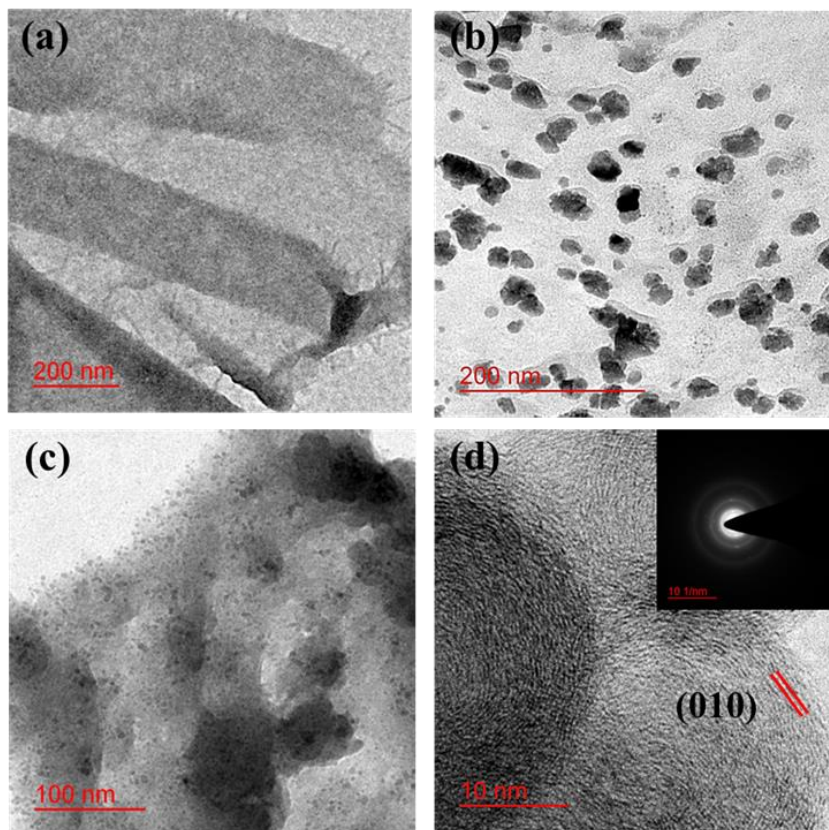
Fig.4.2 TEM image of (a)PBTTT and (b-d)PBTTT/rGO composite FTM film over Cu grid. (d) HR-TEM image of composite film showing (010) plane. The SAED picture of the PBTTT/rGO composite FTM film is seen in the inset.
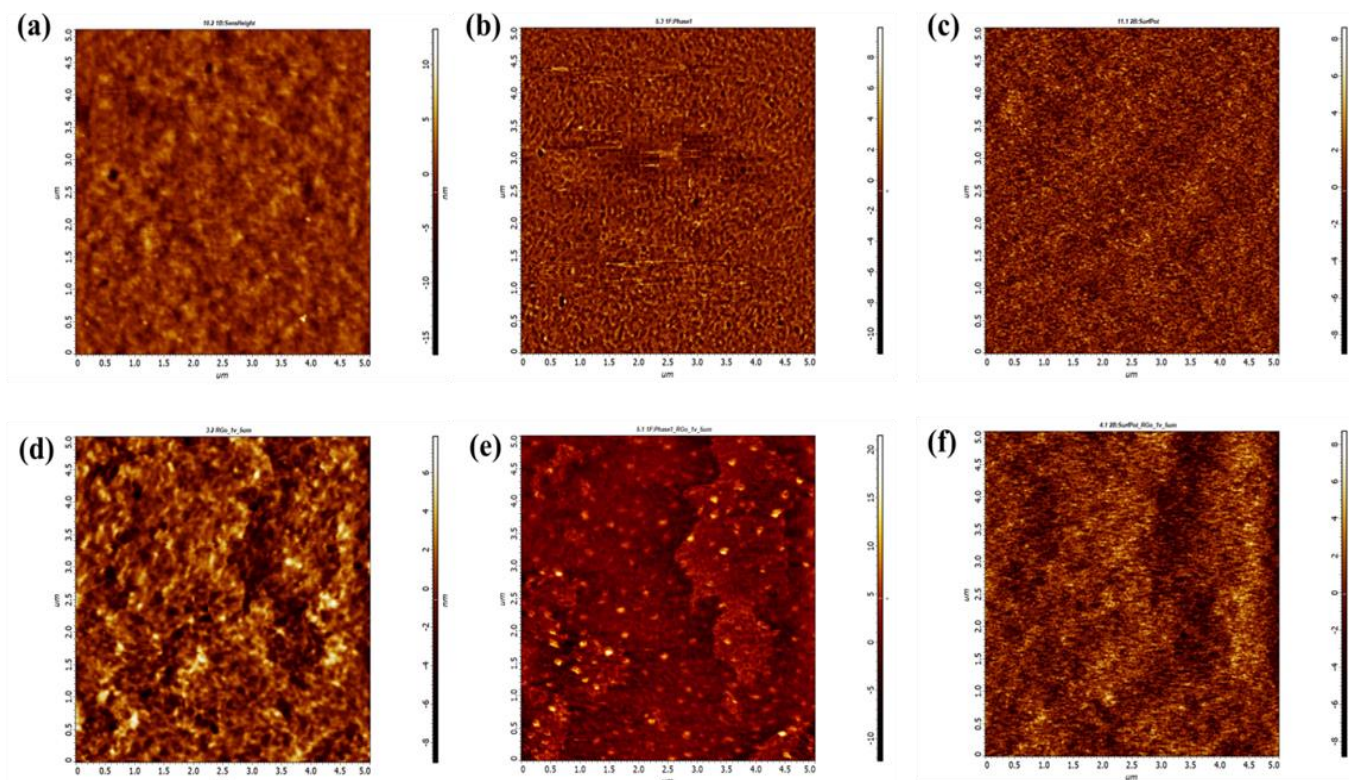
Fig. 4.3 AFM topography, phase image and KPFM image (scan area 5 μ m x 5 μ m) of (a-c) pristine PBTTT FTM film, and (d-f) PBTTT/rGO nanocomposite.

4.2.2.2. Structural Analysis

The out-of-plane XRD of all the films prepared by FTM on the glass substrate is shown in Fig. 4.4.The PBTTT/rGO nanocomposite FTM film exhibits two sets of reflection i.e. (h00) for alkyl stacking of PBTTT chains and (0k0) for π-π stacking with diffraction peaks indexed as (100), (200), (300), (400) and (010) occur at 3.89°, 7.94°, 12.04°, 15.89°and 24.47° respectively. While in the pristine polymer film, the diffraction peaks corresponding to (100), (200), (300), (400) and (010) occur at 4.06°, 8.13°, 12.23°, 15.89° and 24.47° respectively. The peak matching to diffraction planes (100),(200),(300), and (400) for the composite film has moved towards a lower angle compared to pristine film, resulting in a decrease in d-spacing. This change may have occurred as a result of the charge transfer(CT) interaction between the polymer and the filler. It's worth mentioning that the powder XRD of the composite film shows no rGO peak. The presence of rGO in the polymer matrix has been confirmed by a more in-depth morphological investigation.

A relatively modest percentage of nanosheets (3%), which is over the detection threshold, is confirmed here. Peak intensity study of pure PBTTT/rGO using powder XRD displays an increased set of reflections than that of pristine PBTTT film, demonstrating that the formed nanocomposite film produced using the FTM technique allows for the well-growth of polymer nanocomposite domain without thermal treatment. It's worth noting that HR-TEM depicts the (010) plane. However, powder XRD displays both(h00) and (0k0) reflections which (h00) reflections having the highest peak intensity than (0k0) confirming the polymer film's morphology is highly at edge-on orientation. Edge on orientation is sought for OFETs because of the directional nature of mobility (best across either polymer backbone or π-π stacking direction).
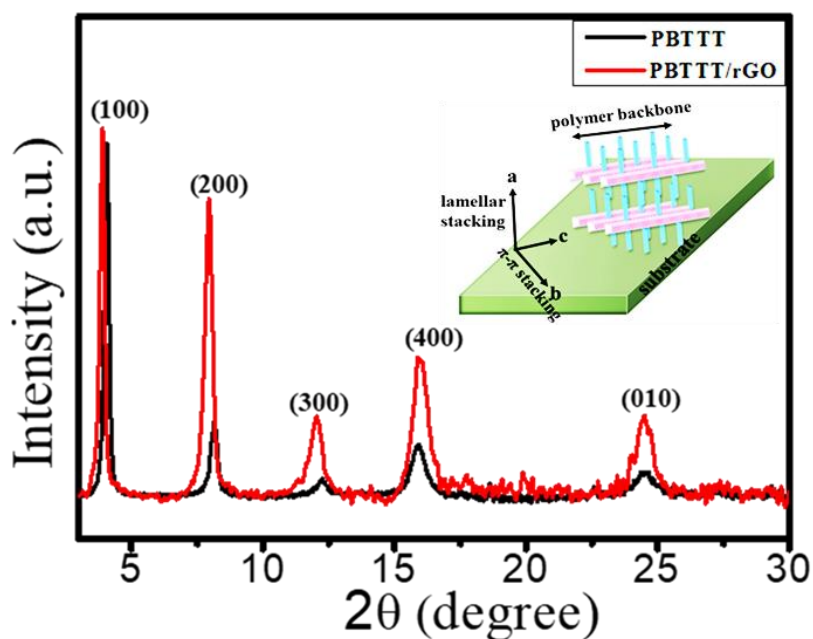

Fig. 4.4 Out of plane XRD of PBTTT and PBTTT/rGO FTM film.

4.2.2.3. Spectral investigation

To investigate the correlations between the polymer and the filler, a UV-Vis and FTIR spectroscopic study was conducted and compared to a pristine sample, as shown in Fig. 4.5. (a & b). Fig. 4.5 (a) shows the normalised spectral response of pure PBTTT films and PBTTT/rGO nanocomposite generated by the FTM method, exhibiting good absorption maxima at 539 nm and 552 nm, respectively, and right shoulder peaks at 587 nm and 595 nm, respectively. The charge transfer (CT) interaction between polymer and rGO is demonstrated by the widening and red shifting of spectra of PBTTT/rGO hybrid films in comparison to pure PBTTT films. Differences in the ratio of vibronic peak intensities (A_{0-0}/A_{0-1}) related to vibronic transition may shift the absorbance spectra toward lower or higher wavelengths, as has been found in the study[287]. Composite films display a red change in their spectral response when compared to the pure PBTTT film, demonstrating the existence of polymer-rGO nanosheet interactions. According to the literature, the amount of polymer aggregation indicating intermolecular interaction can be seen in the absorption bands of thiophene thin films. The red shift in absorption peaks can be explained by interchain and intrachain interactions caused by polymer chain aggregation. Aggregation-induced planarization of the polymer backbone causes red-shifting of optical transitions in these polymer aggregates [288,289,328]. As can be seen in Fig. 4.5(a), the increase in peak ratio occurs as the degree of delocalisation of π-electron and polymer aggregation order increase. For example, it has been shown that rGO may induce polymer chains to produce nanostructures or nanowhiskers via self-assembly [329,291,292]. Because both pristine and composite film was cast using FTM, the increased peak ratio (A_{0-0}/A_{0-1}) is due to the presence of rGO nanosheet in the polymer framework.

The different functionalities present in pure PBTTT and PBTTT/rGO nanocomposite are shown in Fig.4.5(b). The peak at 2971, 2926, and 2881 cm^{-1} have been credited to the asymmetric C–H stretching vibrations present in –CH$_3$, –CH$_2$ groups, and the symmetric C–H stretching vibration present in -CH$_2$ in long alkyl chains of pure PBTTT polymer respectively. The thiophene ring C=C stretching, methyl and methylene deformation of the alkyl chain is responsible for the bands at 1466, 1383,1400 cm^{-1}. The C-S in-plane stretching vibration may be assigned at 817 cm^{-1}. The C–H(in-plane) bending oscillation of the thiophene ring is allocated to the band at 1123 cm^{-1}. In general, the C-H in-plane

bending values in aromatic compounds range from 1000 to 1300 cm^{-1}, while the C-H out-of-plane bending wavenumbers range from 750 to 1000 cm^{-1}. While for PBTTT/rGO nanocomposite, the peak for antisymmetric C–H stretching vibrations that are present in –CH_3 and –CH_2 groups occurs at 2956 cm^{-1}, while the peak for symmetric C–H stretching vibrations that are found in –CH_2 in long alkyl chains occurs at 2920 cm^{-1}. The thiophene ring C=C stretching and methyl deformation of the alkyl chain are at 1464, and 1382 cm^{-1} respectively. The C-S in-plane stretching vibration may be assigned at 809 cm^{-1}. The C–H(in-plane) bending oscillation of the thiophene ring is allocated to the band at 1118 cm^{-1}. All these bands are shifted towards the lower wavenumber in PBTTT/rGO composite. In addition, the peak at 1733 cm^{-1} corresponds to the C=O vibrations from carbonyl groups present in rGO as well as the peak at 1045 cm^{-1} can be attributed to the C-O stretching vibration due to the presence of epoxide groups in the rGO nanosheet which is not visible in the pure polymer. As a result, the FTIR findings demonstrate character trait peaks of both components, indicating that rGO was successfully integrated into the PBTTT matrix [330].
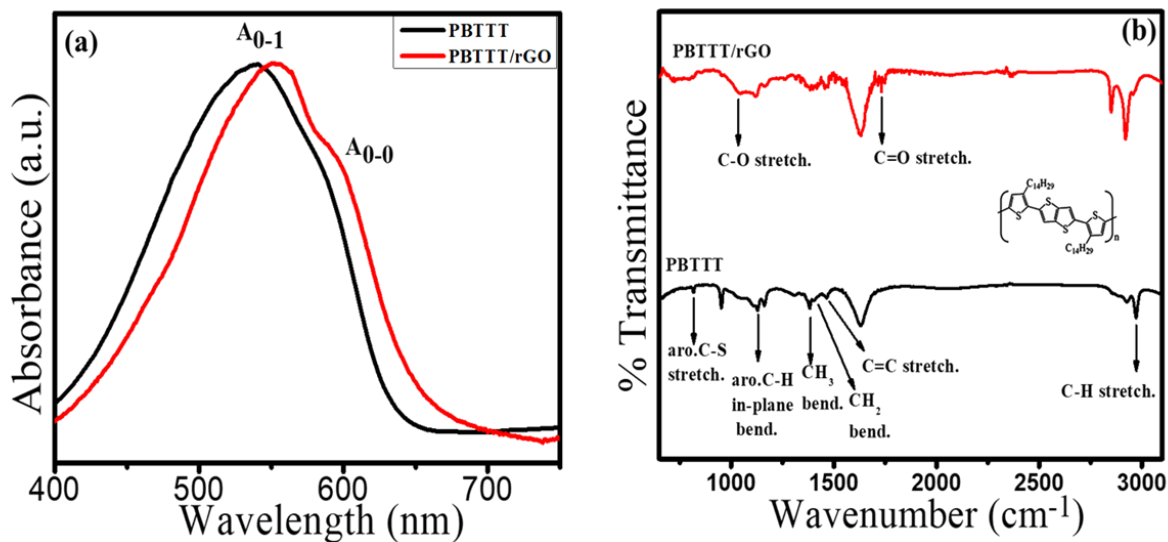
Fig.4.5(a) Normalized spectral response of PBTTT, and PBTTT/rGO nanocomposite FTM film and (b) FTIR spectra of (i) PBTTT and (ii) PBTTT/rGO.

4.2.2.4. Cyclic voltammetry study(CV)

Additionally, CV measurement was explored to evaluate aggregation, charge transfer, as well as the frontier orbital energy levels for both films generated on ITO substrate, as shown in Fig. 4.6. There are notable differences between PBTTT and PBTTT/rGO nanocomposites regarding the general appearance of the anodic(oxidation) peak locations. The lower anodic peak is indicative of the presence of aggregated PBTTT chains, while the higher one is due to the combination of amorphous or a mixture of amorphous and aggregated PBTTT chains [331]. The composite film's HOMO level was determined to be -5.19 eV while the pure polymer film was estimated to be -5.29 eV using the eqn.4.1. When the GO is present, polymer nanostructures formation and charge transfer interactions are induced, resulting in a change in HOMO energy level [332], according to Istif and colleagues. Because of this, the modification of the HOMO level, in addition to the nature of the optical absorption response, is evidence of a change in the electronic distribution of the composite material. There is widespread consensus in the literature that various morphologies exhibit varying levels of energy. The scientific community as a whole seems to agree that different morphologies display different energy levels and work functions of electrons, both of which are directly related to outward appearance and the electrical energy transfer that occurs between polymer chains [293,333]. This assertion has garnered a great deal of attention in the scientific community. CV is also related to the work function of materials since it is the process by which an electron is ejected from the highest occupied frontier orbital to the surface. This process occurs when a material is irradiated. A change in the oxidation peak is produced as a consequence of the fusion of PBTTT with rGO, and this change is completely distinct from the pure polymer peak.

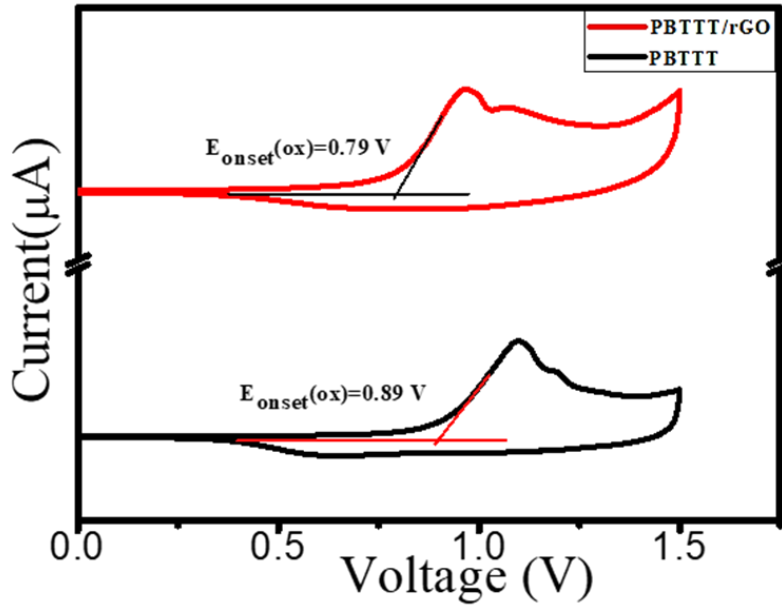$$E_{HOMO} = -e(4.4 + E_{ox}(onset)))V \qquad (4.1)$$

Fig. 4.6 CV of pure PBTTT, and PBTTT/rGO nanocomposite FTM film over ITO-coated glass substrate

### 4.2.2.5. OFET's Characterization

OFET was constructed by depositing top Au electrodes with a channel length of 30 µm and a channel width of 1 mm. This was done so that the charge transport characteristics could be investigated. It should be noted that all synthesis, film deposition, device construction, and measurements were accomplished in the dark at room temperature with a relative humidity of 55%. The well-known p-type I_{DS}-V_{DS} output and I_{DS}-V_{GS} transfer characteristics are evident from the preliminary examination. Figures 4.7(a,b) and (c,d) illustrate the output (I_{DS} and V_{DS}) and transfer (I_{DS} and V_{GS}) characteristics of pristine polymer and nanocomposite film, respectively. In the saturated regime, equation(4.2) was used to compute characteristics like field effect mobility (µ) and the on/off ratio.

$$I_{DS} = \frac{W}{2L}\mu C_i(V_{GS} - V_{th})^2 \qquad (4.2)$$

Where I_{DS} is the drain current, W is channel width and L is channel length, C_i is the capacitance per unit area, and V_{GS} is the injected gate voltage. With this equation, it was established that the average mobility(μ) of the composite film at -40 V was 0.26cm^2/V.s; this was 21.66 times more than pristine polymer (μ=0.012 cm^2/V.s) and more than four times in on/off ratio($\sim$1.3x10^3) under ambient. Taking into mind the surface topography, GIXD, which is where the lamella of PBTTT are being supported synergistically by rGO nanosheets, it is possible to justify the value that was obtained of having great mobility. The surface morphology of rGO sheets lends credence to the notion that decorating with PBTTT polymer with larger domain sizes is appropriate. XRD and HR-TEM pictures, meanwhile, demonstrate the formation of a strongly edge-on organization, self-assembled PBTTT/rGO layer that is suitable for the device having charge carrier movement in a 2-D plane. Because of this, the mutually dependent supported lamella of PBTTT through rGO increases crystallinity while also enabling charge transfer, which ultimately leads to an increase in channel current and thus mobility of the PBTTT/rGO film [334]. In addition, the broadening of the absorption band of the polymer composite in conjunction with a redshift provides further evidence that charge transfer interaction exists between the polymer and the rGO nanosheets, together with an extended intrachain order and molecular planarity. It is important to note that composite materials may have many kinds of conduction routes, which indicates the existence of percolative behaviour [335,336]. This is something that should be taken into consideration. This percolation channel facilitates charge transmission by reducing the impedance of the passage between the source and the drain electrode. The shift in oxidation potential provides insight into the alterations that have taken place in the electrical characteristics as well as the location of the HOMO and LUMO levels. This HOMO level tweaking might potentially increase the transfer efficiency of electric charge between electrodes and conductive polymer, while at the same time contributing to an increase in the charge carrier mobility of the semiconducting material [296].
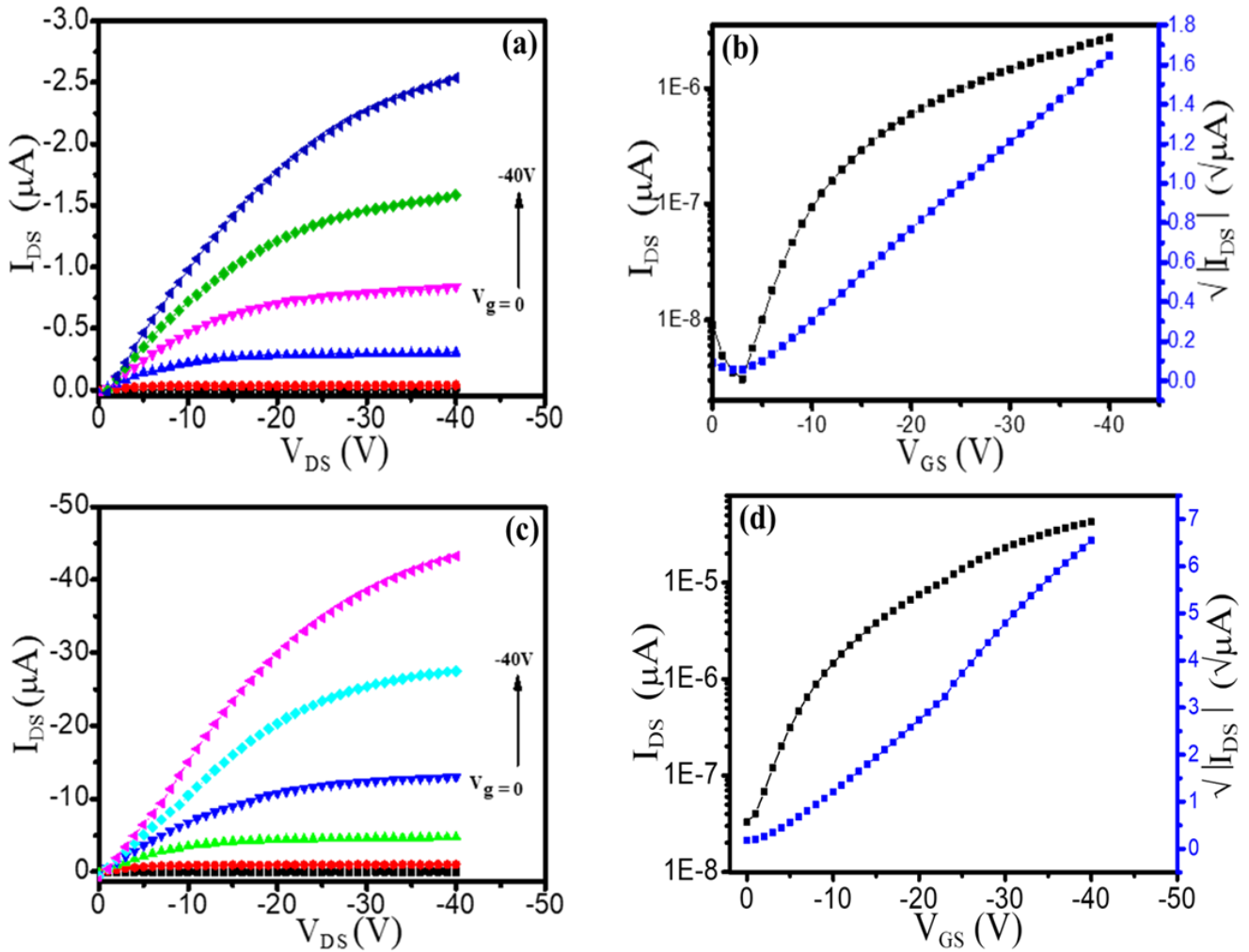
Fig. 4.7 Output (I_{DS}-V_{DS}) and transfer characteristics (I_{DS}-V_{GS}) of (a,b) pristine PBTTT and (c,d) PBTTT/rGO nanocomposite thin film

It is important to note that the performance of OFET is heavily dependent on the symmetrical dissemination of nanomaterials in the polymer matrix. This is something that should be kept in mind. As a consequence of this, we collected the film from 10 distinct sites and measured the I_{DS} -V_{GS} for each of these locations, and the results showed an essentially comparable curve with tiny variations in current, as seen in Fig.4.8.
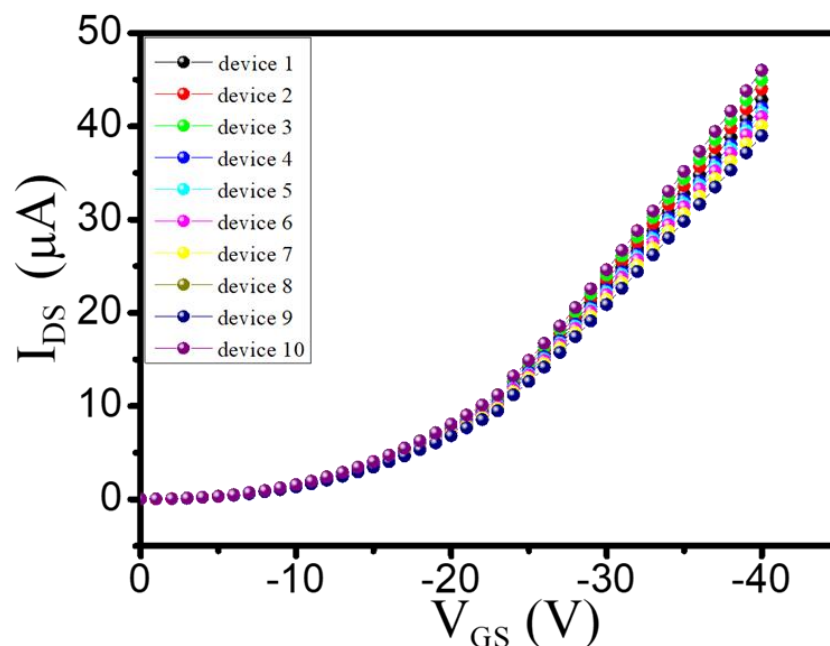
Fig.4.8 I$_{DS}$-V$_{GS}$ transfer characteristics of PBTTT/rGO nanocomposite thin film at 10 different places at V$_{DS}$= -40 V

4.3. Conclusions

Thus, ultrasonication was used to create solution-processable PBTTT/rGO nanocomposites in chloroform. Polymer chains with 2-D rGO nanosheets have dramatically improved long-range ordering and crystallinity. In addition, a simple method for producing self-assembled, highly oriented, anisotropic thin films of PBTTT / rGO nanocomposites was devised using an FTM technique that was based on a liquid base with a high surface free energy. Several different methods of morphological analysis, such as transmission electron microscopy, atomic force microscopy, selected area electron diffraction, and others, demonstrate the production of uniformly dispersed nanosheets, edge-on oriented in a polymer matrix, along with the development of interlinked crystalline regions. This is in comparison to a pure polymer matrix. The UV/vis spectra of pure PBTTT and PBTTT/rGO nanocomposites show that there is an interaction between the polymer and the nanosheets, as well as the ordering of the polymer chains. Also, CV shows how the HOMO level and electrical properties change once the composite film is formed. Finally, an organic field effect transistor (OFET) is

made using a polymer nanocomposite thin film. OFET have better device efficiency in atmospheric conditions, with average field effect mobility of 0.26 $cm^2V^{-1}s^{-1}$ at a drain voltage of -40 V, which is around 22 times that of pristine polymer (μ=0.012 cm^2 /V.s) and more than four times on/off ratio (~1.3 $x10^3$). Our research reveals a method for producing high-quality nanocomposite thin films quickly to increase device efficiency.